Studying the spatial variability of methane flux with five eddy covariance towers of varying height
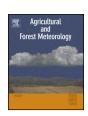
O. Peltola **(University of Helsinki)**
et al

Studying the spatial variability of methane flux with five eddy covariance towers of varying height

O. Peltola [a,*], A. Hensen [b], L. Belelli Marchesini [c], C. Helfter [d], F.C. Bosveld [e], W.C.M. van den Bulk [b], S. Haapanala [a], J. van Huissteden [c], T. Laurila [f], A. Lindroth [g], E. Nemitz [d], T. Röckmann [h], A.T. Vermeulen [b,g], I. Mammarella [a]

[a] *Department of Physics, University of Helsinki, Helsinki, Finland*
[b] *Energy Research Centre of the Netherlands, Petten, The Netherlands*
[c] *Department of Earth Sciences, VU University, Amsterdam, The Netherlands*
[d] *Centre for Ecology & Hydrology, Edinburgh Research Station, Penicuik, UK*
[e] *Royal Netherlands Meteorological Institute, De Bilt, The Netherlands*
[f] *Finnish Meteorological Institute, Helsinki, Finland*
[g] *Department of Physical Geography and Ecosystem Science, Lund University, Lund, Sweden*
[h] *Institute for Marine and Atmospheric Research Utrecht, Utrecht University, Utrecht, The Netherlands*

ARTICLE INFO

ABSTRACT

In this study, the spatial representativeness of eddy covariance (EC) methane (CH_4) measurements was examined by comparing parallel CH_4 fluxes from three short (6 m) towers separated by a few kilometres and from two higher levels (20 m and 60 m) at one location. The measurement campaign was held on an intensively managed grassland on peat soil in the Netherlands. The land use and land cover types are to a large degree homogeneous in the area.

The CH_4 fluxes exhibited significant variability between the sites on 30-min scale. The spatial coefficient of variation (CV_{spa}) between the three short towers was 56% and it was of similar magnitude as the temporal variability, unlike for the other fluxes (friction velocity, sensible heat flux) for which the temporal variability was considerably larger than the spatial variability. The CV_{spa} decreased with temporal averaging, although less than what could be expected for a purely random process ($1/\sqrt{N}$), and it was 14% for 26-day means of CH_4 flux. This reflects the underlying heterogeneity of CH_4 flux in the studied landscape at spatial scales ranging from 1 ha (flux footprint) to 10 km² (area bounded by the short towers). This heterogeneity should be taken into account when interpreting and comparing EC measurements. On an annual scale, the flux spatial variability contributed up to 50% of the uncertainty in CH_4 emissions. It was further tested whether EC flux measurements at higher levels could be used to acquire a more accurate estimate of the spatially integrated CH_4 emissions. Contrarily to what was expected, flux intensity was found to both increase and decrease depending on measurement height. Using footprint modelling, 56% of the variation between 6 m and 60 m CH_4 fluxes was attributed to emissions from local anthropogenic hotspots (farms). Furthermore, morning hours proved to be demanding for the tall tower EC where fluxes at 60 m were up to four-fold those at lower heights. These differences were connected with the onset of convective mixing during the morning period.

1. Introduction

Some 14% of European peatlands are used for agricultural purposes; this number can be as high as 85% in countries with high population density, such as the Netherlands (Joosten and Clarke, 2002). CH_4 fluxes show significant spatial variability, especially in agricultural areas on peat soils (Hendriks et al., 2010; Schrier-Uijl et al., 2010a, 2010b; Teh et al., 2011), due to heterogeneous soil moisture conditions, agricultural management practices and vegetation composition. For instance Hendriks et al. (2010) found up to 25-fold differences in CH_4 fluxes between measurement locations in a single abandoned peat meadow, using chamber systems. This variability was explained by differences in soil water level in combination with root depth patterns and presence of aerenchymatous plant species. High spatial variability of the flux complicates upscaling, since it is difficult to assess how representative of the

wider geographic area measurements are. Upscaling is essential if measurements are to be extrapolated to continental and global CH_4 budgets. Upscaled CH_4 emissions tend to have large uncertainties (Kirschke et al., 2013; Schulze et al., 2009) and agreement with other large scale flux estimation methods (e.g. so-called top-down estimates obtained with inverse modelling) is unsatisfactory at continental (Schulze et al., 2009) and global scales (Kirschke et al., 2013). CH_4 flux spatial variability is often found to be related to spatial variability of water table level and plant communities (Hendriks et al., 2010; Lai et al., 2014), whereas the most important driver for seasonal variability is soil temperature (e.g. Rinne et al., 2007; Yvon-Durocher et al., 2014). In addition, temporal and spatial variability can be caused by ebullition (Tokida et al., 2007) and plant-aided transport (Hendriks et al., 2010; Kim et al., 1999). Plant-aided transport may be passive via diffusion (e.g. Henneberg et al., 2012) or active via convective through-flow through the aerenchyma (e.g. Hendriks et al., 2010; Kim et al., 1999). Generally only a fraction of CH_4 produced in the anoxic conditions is released to the atmosphere, since most of the produced CH_4 is oxidised while it is transported through the oxic zone in the soil (e.g. Le Mer and Roger, 2001).

CH_4 flux spatial variability has been studied at the field scale with a combination of chamber and short tower eddy covariance (EC) measurements, providing information on fluxes at different spatial scales, e.g. chambers on plot scale ($\sim 1\,m^2$) and EC on ecosystem scale (~ 1 ha) (e.g. Hendriks et al., 2010; Schrier-Uijl et al., 2010b; Teh et al., 2011). Schrier-Uijl et al. (2010b) and Hendriks et al. (2010) found 13% and 37% differences in long term CH_4 budgets between the fluxes obtained with these techniques, respectively, at two Dutch peat meadow sites. Even though the agreement between the methods was reasonable, it is difficult to assess how well they scale up to larger spatial areas, i.e. how representative the obtained CH_4 flux estimate at the field scale is for the whole landscape (>1 km^2).

The objective of this study was to assess the CH_4 emissions at spatial scales which fall between the regular EC towers (field scale, ~ 1 ha) and inverse modelling (~ 100–$500\,km^2$). At the same time this study assesses the application of installing EC measurements on tall towers established for the concentration monitoring needed for the inverse modelling in order to simultaneously provide information on emissions at the regional and at the landscape scale. Such studies could help bridge the gap between these two methods and may help understand why bottom-up and top-down estimates for large scale CH_4 emissions often disagree. During the measurement campaign the spatial variability of CH_4 emission in an agricultural peatland landscape in the Netherlands was investigated with three short eddy covariance towers, separated by a few kilometres, and one tall tower which integrated CH_4 emissions from a larger area. It was hypothesised that the tall tower averages out the CH_4 flux variability seen with the three short towers, providing the integrated flux from the studied landscape to the atmosphere. Multilevel EC measurements allowed the spatial variability of CH_4 flux to be studied in the surrounding landscape, since the size of the source area of the flux, i.e. flux footprint, increases with measurement height (e.g. Rannik et al., 2012). Footprint modelling (Kljun et al., 2002, 2004) was used for spatial apportionment of observed fluxes and their comparison with known distributions of local sources of CH_4. Differences in spatial scales between tall tower and short towers were also investigated.

2. Materials and methods

The present study was supported by an EU FP7 infrastructure project InGOS (Integrated non-CO_2 Greenhouse gas Observing System) and was held 1–25 July 2012 in the surroundings of the Cabauw Experimental Site for Atmospheric Research (CESAR). It was a follow-up campaign to a CH_4 flux instrument intercomparison campaign which was held during June 2012. Results from the intercomparison experiment have been summarised elsewhere (Peltola et al., 2014); the same instruments were used in this study.

2.1. Site description

2.1.1. Landscape characteristics

The CESAR site (51°58′12.00″ N, 4°55′34.48″ E, −0.7 m a.s.l) is located in the "Groene Hart" (i.e. Green Heart) of the Netherlands. Compared to other parts of the country, this area is relatively sparsely populated and largely used for agriculture, predominantly dairy farming.

The landscape comprises polders separated by dikes. Polder areas consist of large numbers of rectangular fields with drainage ditches running between them (see Fig. 1a). The fields are mostly intensively managed grasslands used as pasture and for growing hay and livestock fodder (e.g. maize (*Zea mays*)). Based on Beljaars and Bosveld (1997) the dominant grass species in the area are *Lolium perenne*, *Poa trivialis*, and *Alopecurus geniculatus*. The area is flat with no apparent slopes or hills and thus it is ideal for micrometeorological measurements. The farms in the area were located close to each other and were lined up between the fields (Fig. 1a). Cattle were the main type of livestock in the area, however sheep, pigs, poultry, rabbits, turkeys and horses were also present. Statistics on the main livestock categories are given in Table 1.

The soil consists mostly of river clay and peat, with peat fraction increasing with distance from the nearby river Lek. All EC measurements in this study were located in an area where the soil was classified as soil profile type Rv01C or 'Drechtvaaggrond' in the Dutch soil classification system (Wösten et al., 2001). This soil class is characterised by a few tens of centimetres thick layer of clay which overlays a deep peat layer. Soil profiles measured at the CESAR site by Jager et al. (1976) showed that the top 0.60 m consisted mostly of clay (8–12% organic matter with high root density), 0.60–0.75 m depth was a mixture of clay and peat (1–3% organic matter with low root density) and a peat layer extended from 0.75 m to 7.00 m below the surface. Most of the (grass) roots were confined to the top 0.18 m deep layer.

The water table depth is actively monitored and controlled in several locations within the polder area (Fig. 1). Water is pumped out of the polder and into the river Lek (a tributary of the Rhine river) if the level exceeds a preset threshold. During dry spells in summer, this drainage may be reversed by letting in water from the river. The water level in the ditches is maintained at on average about 0.4 m below the surface (Beljaars and Bosveld, 1997). In previous studies conducted in similar ecosystems during summer time, drainage ditches and ditch edges have been observed to be CH_4 emission hotspots (Hendriks et al., 2010; Schrier-Uijl et al., 2010b), whereas the central parts of the fields were not such significant CH_4 emitters due to the fact that the water level in the soil depends on the distance from the closest drainage ditch.

2.1.2. CESAR site

2.1.2.1. Site description.
The vegetation at the CESAR site itself was dominated by grasses (*Lolium perenne* (55%), *Festuca pratense* (15%), and *Phleum pratense* (15%)) (Beljaars and Bosveld, 1997). During the campaign, tussocks of *Juncus effusus* were observed in the fields and especially on edges of the drainage ditches. *J. effusus* may act as a conduit for diffusive transport of CH_4 within its aerenchyma (Henneberg et al., 2012; Schäfer et al., 2012), thereby thus potentially increasing the efflux of CH_4 to the atmosphere. Next to the CESAR 6 m tower, which was located 87 m away from the main mast (213 m high tall tower, see Fig. 1b), maize (*Z. mays*) was grown in two fields in the 180–280° wind sector. This was the prevailing
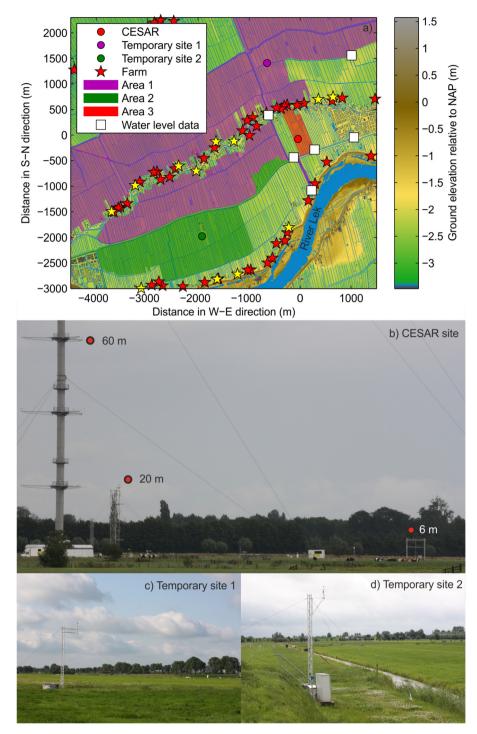
Fig. 1. The topmost part of the figure (a)) shows an overview of the landscape. The colour shows the ground elevation (dark grey: buildings/elevation data not available; blue: water surface) relative to Normal Amsterdam Level (NAP) (AHN-2, www.ahn.nl). Yellow stars show farms with more than 100 cows. Water level in the ditches was controlled in three different areas separately from each other (Area 1, 2 and 3). The picture in the middle (b)) shows the measurement setup at the CESAR site (picture was taken towards SE, red circles show EC measurement locations) and the two pictures at the bottom (c) and d)) show the measurement setup at the two temporary sites (pictures were taken towards SW and S-SW, respectively).

wind direction during the campaign and thus the CH_4 exchange of these maize fields was often observed with the CESAR 6 m system. For more information about the site, see Beljaars and Bosveld (1997) and Van Ulden and Wieringa (1996).

2.1.2.2. Measurements at the site. Ecosystem scale CH_4 fluxes were obtained by EC at three heights at the CESAR site (6 m, 20 m and 60 m aboveground). The "Fast Greenhouse Gas Analyzer" (FGGA, Los Gatos Research Inc., USA) was used to acquire 10 Hz measurements of CH_4, CO_2 and H_2O mole fractions at 60 m height (Table 2). The analyser was coupled with a Gill R3 (Gill Instruments Ltd, UK) ultrasonic anemometer used for the measurement of the turbulent fluctuations of 3D wind components and sonic temperature. A 12 m long sampling line (PTFE, inner diameter: 9 mm) was used to

Table 1
Statistics of the livestock raised on the farms which were affecting the EC fluxes based on footprint analyses. The emissions factors (EF) used in the bottom-up approach (Eq. (4)) for each animal category are also provided.

Category	N	Average N per farm	EF (kg(CH_4) year^{-1} head^{-1})	EF uncertainty (%)
Mature dairy cattle	2892	69	126	15
Mature non-dairy cattle	1355	40	73	20
Young cattle	419	84	34	20
Sheep	946	50	8	30
Swine	709	142	1.5	30
Horse	61	8	10	30

sample air for the gas analyser. The sampling line inlet was located approximately 30 cm below the sonic head.

The eddy covariance system at the 20 m height consisted of two gas analysers a cavity ring-down analyser (G1301-f, Picarro Inc., USA) and a "Fast Methane Analyzer" (FMA, Los Gatos Research Inc., USA) and one ultrasonic anemometer (Windmaster Pro, Gill Instruments Ltd, UK) (Table 2). The G1301-f measured mole fractions of CH_4 and CO_2, whereas the FMA measured CH_4 and H_2O. The two analysers sub-sampled off a shared 22 m long main inlet line (PTFE, inner diameter: 9 mm). The inlet was situated approximately 20 cm below the anemometer. After the flux data processing steps (see Appendix A) the two CH_4 flux systems at the 20 m height produced comparable results ($F_{FMA} = (0.998 \pm 0.005)F_{G1301-f} + (1.11 \pm 0.25)$ nmol m^{-2} s^{-1}, RMSE = 3.6 nmol m^{-2} s^{-1}, $r^2 = 0.99$) and thus in order to maximise the data coverage their data were combined into one dataset.

At 6 m height, a G2311-f (Picarro Inc., USA) and a USA-1 anemometer (METEK GmbH, Germany) were used to measure CH_4, CO_2 and H_2O dry mole fractions, the three orthogonal wind components and sonic temperature, respectively (Table 2). A 30 m long heated PTFE sampling line (inner diameter: 8 mm) was used to sample air for the G2311-f. The measurement setup at 6 m height was exactly the same as used in Peltola et al. (2014) for G2311-f. The 6 m mast at the CESAR site was located 87 m WSW (250°) from the CESAR site 213 m high tall tower, and the tower used for 20 m level measurements was located approximately 20 m towards SSE (170°) (Fig. 1b).

Variation in the boundary layer height (BLH) during the campaign was retrieved by a ceilometer (LD-40, Vaisala Oyj, Finland) using the wavelet algorithm of De Haij et al. (2007). The algorithm is able to estimate BLHs between 90 and 3000 m, with 7.5 m resolution. Gaps in the 10 min BLH data were filled with linear interpolation if the gap was short (less than 1 h), whereas longer gaps where filled with the mean diel variation. Vertical profile (20 m, 60 m, 120 m and 200 m) of CH_4 dry mixing ratio was measured with G2301 (Picarro Inc., USA) on the main mast. The instrument was routinely calibrated against the NOAA2004 concentration scale and the sample air was dried with a cryo trap drier at $-40\,°C$ before entering the gas analyser. In order to increase the vertical resolution of the CH_4 dry mixing ratio measurements, the values recorded with the EC gas analyser at 6 m height (G2311-f) were combined with the G2301 data and used to estimate the changes in the CH_4 vertical profile for storage calculations. Meteorological variables were recorded at the CESAR site by a standard weather station run by Royal Netherlands Meteorological Institute (KNMI).

2.1.3. Temporary site 1
2.1.3.1. Site description. Temporary site 1 (51.983054° N, 4.916738° E) was located next to a drainage ditch, approximately 1600 m away from the CESAR site in direction 335° (see Fig. 1a). The vegetation at the site was dominated by grasses, and some stinging nettle (*Urtica dioica*) was growing next to the drainage ditches. A maize (*Z. mays*) field was located approximately 200 m away in direction 240°. Occasionally cattle from a nearby

Table 2
Description of the measurement system at each EC measurement location.

Site	Measurement height (m)	Roughness length (m)	Gases measured	Sonic anemometer	Gas analyser	τCH_4[a] (s)	Filters	Pump
CESAR	60	Wind direction dependent	CH_4, CO_2, H_2O	R3	FGGA	0.22	Coarse dust (inlet) + 10 µm particulate filter	Dry vacuum scroll pump (XDS35i, BOC Edwards, Crawly, UK)
	20	Wind direction dependent	CH_4, CO_2, H_2O	Windmaster Pro	FMA & G1301-f	0.2 & 0.2	Coarse dust (inlet) + Whatman glass fibre thimbles, 603G+ 2 µm Swagelok (Swagelok pat no. SS-4FW4-2)	Vacuum scroll pump (Varian TriScroll 300, Palo Alto, California, USA)
	6	0.03	CH_4, CO_2, H_2O	USA-1	G2311-f	0.45	Coarse dust (inlet) + 10 µm particulate filter	Side channel blower (Samos SB 0080D, Busch Produktions GmbH, Maulburg, Germany)
Temporary site 1	6	0.03	CH_4, CO_2, H_2O	USA-1	FMA & LI-7000	0.12	Coarse dust (inlet) + 2 µm Swagelok (Swagelok pat no. SS-4FW4-2)	Dry vacuum scroll pump (XDS35i, BOC Edwards, Crawly, UK)
Temporary site 2	6	0.03	CH_4	Windmaster Pro	DLT-100	0.17	60 µm Coarse dust (inlet) + 2 µm Swagelok (Swagelok pat no. SS-4FW4-2)	Dry vacuum scroll pump (XDS35i, BOC Edwards, Crawly, UK)

[a] Empirical response time used in correcting CH_4 fluxes for lowpass filtering effects.

farm were grazing in the surroundings of the measurement mast, particularly in the 10–40° and 170–180° wind sectors. Periods when the grazing cows were affecting the EC CH_4 measurements were detected and screened using the method presented in Appendix A.

2.1.3.2. Measurements at the site. The FMA (Los Gatos Research Inc., USA) was used to measure CH_4 mole fractions, and CO_2 and H_2O were measured with a LI-7000 (LI-COR Biogeosciences, USA) (Table 2). Both analysers were measuring at 10 Hz. Fast measurements of the three orthogonal wind components and of (sonic virtual) air temperature were made with a USA-1 ultrasonic anemometer (METEK GmbH, Germany). The anemometer was located at the top of a 6 m high mast and the gas analysers were sampling approximately 20 cm below the anemometer (see Fig. 1c). FMA and LI-7000 sub-sampled off a common inlet line (inner diameter: 9 mm, length: 8 m, material: PTFE). The line was not heated and the samples were not dried. H_2O measured with the LI-7000 was used to correct the FMA CH_4 mole fractions for the dilution and spectroscopic effects (see Peltola et al. (2014) for the correction procedure used).

2.1.4. Temporary site 2
2.1.4.1. Site description. Temporary site 2 was located at 51.952457° N, 4.898425° E, approximately 2800 m SW (direction: 220°) away from the CESAR site (Fig. 1a). The vegetation at Temporary site 2 consisted mostly of grasses, with some *Phragmites australis* was observed next to the drainage ditches. *P. australis* has been shown to transport CH_4 effectively to the atmosphere via its aerenchyma (e.g. Kim et al., 1999).

2.1.4.2. Measurements at the site. A DLT-100 (Los Gatos Research Inc., USA) was used to measure CH_4 mole fractions at Temporary site 2, whereas the three orthogonal wind components and (sonic virtual) air temperature were measured with a Windmaster Pro (Gill Instruments Ltd, UK) ultrasonic anemometer (Table 2). Both instruments provided data with 10 Hz frequency. A PTFE sampling tube (length: approx. 10 m, inner diameter: 9 mm) was used to sample air for the CH_4 analyser. The inlet of the sampling line was situated approximately 15 cm below the anemometer. Since the DLT-100 was not connected to a drier and H_2O was not measured at the site, it was not possible to correct the CH_4 fluxes for dilution and spectroscopic effects that the H_2O has on the measured CH_4 (e.g. Peltola et al., 2014). Thus, the CH_4 fluxes at this site are slightly underestimated (less than 1 nmol m^{-2} s^{-1}). For further discussion about the H_2O correction, see Peltola et al. (2014).

2.2. Eddy covariance data processing

Eddy covariance data were post-processed with the EddyUH software (freely available at https://www.atm.helsinki.fi/Eddy_Covariance/EddyUHsoftware.php). Data were post-processed in a similar manner as in Peltola et al. (2014) and thus the steps will only briefly be described in Appendix A.

In order to make the EC fluxes at different heights more comparable with each other, the storage change term ($F_{CH_4}^{STO}$) was added to the turbulent fluxes ($F_{CH_4}^{EC}$):

$$F_{CH_4} = F_{CH_4}^{EC} + F_{CH_4}^{STO}. \tag{1}$$

If not stated otherwise, the sum of the turbulent flux ($F_{CH_4}^{EC}$) and storage change term ($F_{CH_4}^{STO}$) are referred to as 'flux' and marked with F_{CH_4} or with $F_{CH_4}^{EC} + F_{CH_4}^{STO}$. The storage change term takes into account the accumulation (or venting) of CH_4 (or any other scalar) below the EC measurement level (Foken et al., 2012). In this manner

the surface flux is derived. The storage change term was calculated using the CH_4 dry mixing ratio profile measured at the CESAR site (see Section 2.1.2) and the values ranged between −11 and 15 nmol m^{-2} s^{-1} at 60 m level, between −5 and 5 nmol m^{-2} s^{-1} at 20 m level and between −2 and 2 nmol m^{-2} s^{-1} at 6 m level. The reported values are 25th and 75th percentiles of the calculated storage change term time series.

2.3. Assessing landscape level flux variance

In order to study the significance of CH_4 flux spatial variability, the landscape scale variance (total variance σ_{tot}^2) was estimated using data from the three short towers and was divided into spatial and temporal components (after Sun et al. (2010)) as

$$\sigma_{tot}^2 = \frac{m(n-1)}{(m*n)-1}\bar{\sigma}_s^2 + \frac{n(m-1)}{(m*n)-1}\sigma_t^2(\mu) \equiv \sigma_{spa'}^2 + \sigma_{tem}^2, \tag{2}$$

where m is the number of temporal data points, n is the number of measurement locations, $\bar{\sigma}_s^2$ is the time-averaged spatial variance (variance between the three measurement locations calculated for each time step and then averaged over time) and $\sigma_t^2(\mu)$ is the temporal variance of the spatially averaged flux time series (μ). However, apparent spatial variability may also be caused by differences between instruments and thus the estimated spatial variance ($\sigma_{spa'}^2$) is divided into the "real" spatial variance (σ_{spa}^2) and instrument related variance (σ_{ins}^2) by assuming that these two sources of variance are not correlated:

$$\sigma_{tot}^2 = \sigma_{spa}^2 + \sigma_{ins}^2 + \sigma_{tem}^2. \tag{3}$$

The first term on the right hand side of the equation ($\sigma_{spa}^2 = \sigma_{spa'}^2 - \sigma_{ins}^2$) describes the variance related to spatial variations, the second term (σ_{ins}^2) represents the variance caused by the differences between instruments and the third term (σ_{tem}^2) describes the variance related to temporal variations in spatially averaged means. For reasons of simplicity σ_{spa}^2 is called spatial variance, σ_{tem}^2 temporal variance and σ_{ins}^2 instrument related variance. σ_{ins}^2 were estimated using the data obtained during the campaign when the used flux instruments were measuring at the same location for approximately one month (Peltola et al., 2014). It should be noted that σ_{spa}^2 contains a contribution of the true variance between sites as well as a contribution of the stochastic nature of turbulence at a single site (site internal spatial variability). The temporal variability can be assessed from measurements at one tower, whereas for estimating the spatial variability several towers are needed. Thus, the relative magnitude of these variance components describes how well one short eddy covariance tower is representative of the whole landscape.

The coefficient of variation ($CV = \sigma/|F|$, where F is spatially and temporally averaged flux) was calculated using the variances above and was used to interpret the results. It is worth noting that the CV calculated using σ_{spa} is similar to the coefficient of spatial variation used in Katul et al. (1999) and Oren et al. (2006). They assessed the spatial variability of CO_2 and other turbulent fluxes with six towers above a loblolly pine forest plantation. However, their study was conducted within roughness sublayer, while this study examines fluxes above this layer.

The flux variance was partitioned for 30-min averaged and long-term mean fluxes (Sections 3.4.1 and 3.4.2). Further, the contribution of the flux spatial variability on the uncertainty of the annual CH_4 balance was estimated by combining these results with three years of CH_4 fluxes presented earlier by Kroon et al. (2010). They measured CH_4 exchange at a site called Oukoop, which is located approximately 12 km to the NW from the study site. It is situated in similar surroundings, i.e. intensively managed grassland polder on peat and thus the spatial variability estimated in

this study is applicable to the Oukoop measurements. The annual uncertainty estimates were calculated using the method presented in Appendix B and are presented in Section 3.4.3.

2.4. Estimating emissions of CH_4 from the nearby farms

Several farms were located in the experimental area (Fig. 1a). Information about the farms (location, animal numbers in different categories) was obtained from www.nationaalgeoregister.nl. Mostly these farms were dairy farms, although some beef cattle, sheep, swine and horses were also present (Table 1). Bottom-up estimates (BUE) for each farm's CH_4 emissions were calculated by multiplying the number of animals in each category with the corresponding CH_4 emission factor. The emission factors were taken from the Dutch National Inventory Report 2014 (Coenen et al., 2014). Only CH_4 emissions from enteric fermentation were taken into account, since no information about the amount of stored manure or about the storage method were available. Emission factors for stored manure depend strongly on the storage method: they range between 36% and less than a percent of the emission factor for enteric fermentation of a mature dairy cattle (Pattey et al., 2005). Thus including them in the bottom-up estimate might bias the result.

In order to be able to compare the bottom-up estimated farm CH_4 emissions with the calculated CH_4 fluxes, Eq. (C.1) (see Appendix C) was discretized and the farm emissions were multiplied with the value of the footprint function at the grid cell of each farm:

$$F_{\text{farm}}(0, 0, z_m) = \sum_i \sum_j f_{\text{farm}}(x_i, y_j, 0)\phi(x_i, y_j, z_m),\qquad(4)$$

where F_{farm} is the BUE for the effect of farm CH_4 emissions on the estimated EC flux, $f_{\text{farm}}(x_i, y_j, 0)$ is the CH_4 emission based on emission factors from a farm located at point $(x_i, y_j, 0)$, $\phi(x_i, y_j, z_m)$ is the weighted contribution of the land area located at $(x_i, y_j, 0)$ to the total flux measured at $(0, 0, z_m)$. The above equation gives the farm emission estimate F_{farm} as flux density, since it is already divided with the grid pixel size ($\Delta x \Delta y = 9 \text{ m}^2$).

Top-down estimates (TDE) for the farm CH_4 emissions were obtained by assuming that (1) F_{CH_4} at 6 m height at the CESAR site were not affected by the farms (i.e. the flux originates only from the soil) and (2) the 6 m level CH_4 fluxes are representative of soil emissions of CH_4 within the flux footprint at the 60 m level. After these assumptions the farm CH_4 emissions within the 60 m level footprint can be assumed to be equal to $F_{CH_4,60\,\text{m}} - F_{CH_4,6\,\text{m}}$, although emissions from stored manure may complicate this comparison. Comparison between the BUE and TDE CH_4 emissions is presented in Section 3.6.

3. Results

3.1. Meteorological conditions during the campaign

Daytime temperatures ranged between 10.6 °C and 28.3 °C (on average 18.2 °C) and precipitation as rain was observed for 16 out of 25 days (Fig. 2). 14th of July was the rainiest day (28.7 mm) and the overall precipitation during the campaign was 104.5 mm. Wind speed was on average 3.9 m s^{-1} and the most common wind direction was SW.

Maximum daytime sensible and latent heat fluxes were approximately 115 and 263 W m^{-2}, respectively, and the midday (between 11:00 and 14:00 local time) Bowen ratios were approximately 0.40 and 0.35 for CESAR 6 m and Temporary site 1 locations, respectively (Fig. 3). During most nights wind speeds drops and a stable surface layer develops, with negative sensible heat flux and latent

heat flux close to zero. Night time BLH was around 200–400 m, and BLH started to increase in the morning, reaching maximum levels of approximately 1200–1500 m in the afternoon, lagging a couple of hours after the maximum in energy fluxes. The water table depth stayed relatively constant during the campaign at the three different areas (Fig. 2): at area 3 (around CESAR site) it was on average −0.2 m, whereas at area 1 (around Temporary site 1) and area 2 (around Temporary site 2) it was −0.6 m.

3.2. Footprint size and flux source area characteristics

Fig. 4 shows the footprint climatology and CH_4 flux wind direction dependence for each measurement location. At all locations the footprints were often directed towards W–SW, which was the prevailing wind direction during the measurement campaign. The footprint maximum for the short towers was on average 80 m away and 80th percentile was 250 m away (80% of the measured signal originated from closer than this distance). Site-specific values are given in Table 3. The footprint sizes were very similar between the three short towers, which are reasonable since the variables controlling the size (measurement height, surface roughness, wind, atmospheric stability) were similar.

The three level EC measurement system at the CESAR site provided CH_4 fluxes with different spatial averaging as shown by the unequal footprint sizes (Table 3 and Fig. 4) increasing with the measurement height. For 60 m fluxes the 80th percentile was on average 2000 m away from the measurement point where as for the 20 m and 6 m level fluxes this distance was on average 680 m and 260 m, respectively.

It has been recognised in several papers that in this kind of landscape the CH_4 emission rate to the atmosphere in summer is likely to depend on the distance from the drainage ditch (Hendriks et al., 2010; Schrier-Uijl et al., 2010b) and the measurement area is often divided into three categories: field, ditch edge and ditch. Based on Hendriks et al. (2010) and Schrier-Uijl et al. (2010b) the highest CH_4 emissions were observed on the ditch edge, followed by the ditch and the field area. The differences in CH_4 emission rates are related to differences in water table position in these three surface categories. The footprint-weighted fractions of these three landscape elements at the three measurement locations are given in Table 3. The field fractions were around 0.8 at the three short tower sites, meaning that on average 80% of the CH_4 flux originated from the fields, ditch edge and ditch fractions were on average 0.13 and 0.09, respectively. The largest fraction of ditch area within the footprint was observed at Temporary site 1 where the measurement tower was located next to a drainage ditch. CH_4 emissions at this site were larger in the direction of the ditch (see Fig. 4), compared to areas where drier field conditions prevailed. However, the largest CH_4 emissions observed at the short towers were found at the CESAR 6 m site. This was most likely related to differences in water table height between sites (see Fig. 2d). The three landscape components (field, ditch and ditch edge) were represented in a similar way at the three measurement heights (Table 3) and thus the five EC systems were sampling fluxes from similar areas.

3.3. Average CH_4 flux levels and diel patterns

Out of the three short tower measurement locations Temporary site 2 showed usually lowest CH_4 emissions (median: 24 nmol m^{-2} s^{-1}), followed by Temporary site 1 (30 nmol m^{-2} s^{-1}) and CESAR 6 m (36 nmol m^{-2} s^{-1}) (Fig. 3b). The Kruskal–Wallis test was used to test whether the F_{CH_4} at the three sites could be attributed to the same spatial distribution, i.e. the variation observed between the sites is purely random. The autocorrelation in the three CH_4 flux time series was taken into account by using the variance inflation factor (e.g. Wilks, 2006). Based on the
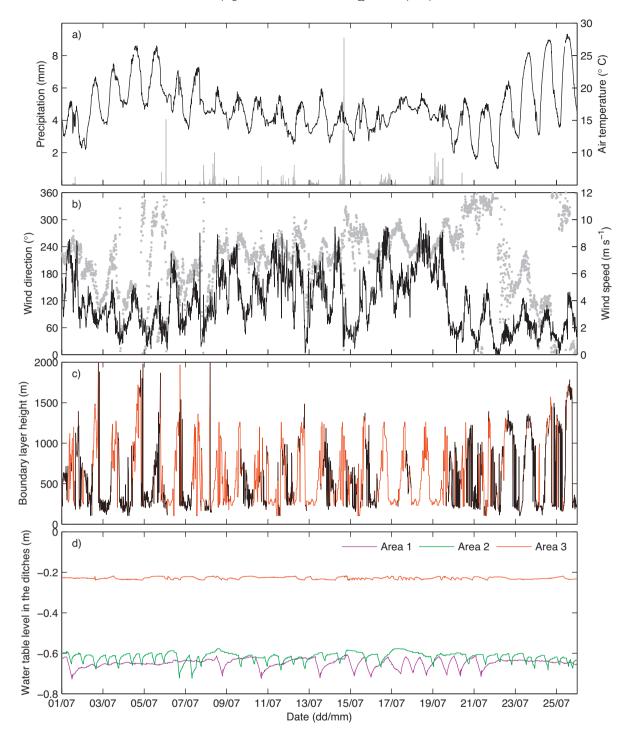
Fig. 2. Meteorological conditions during the measurement campaign. (a) Air temperature (black line) and precipitation with 10 min interval (grey bars). (b) Wind speed (black line) and direction (grey dots). (c) Boundary layer height (black = measurements, red = gap-filling). (d) Water table level in the ditches (relative to ground level) at different parts of the landscape (see Fig. 1) (For interpretation of the references to colour in this figure legend, the reader is referred to the web version of this article.).

Table 3
Statistics of the footprint size and land cover type within the footprint.

Site	Footprint			Land cover fraction[b]		
	Maximum (m)	80th percentile (m)	Area[a] (10^4 m^2)	Field	Ditch	Ditch edge
CESAR 60 m	810	2000	104	0.76	0.09	0.11
CESAR 20 m	240	680	16	0.78	0.09	0.12
CESAR 6 m	90	260	2	0.82	0.07	0.12
Temporary site 1	80	240	2	0.74	0.11	0.11
Temporary site 2	90	250	3	0.75	0.08	0.17

[a] Area within the 80th percentile curve on average.
[b] Land cover fractions do not sum up to unity, since occasionally there were also buildings, roads, river Lek etc. within the footprint.
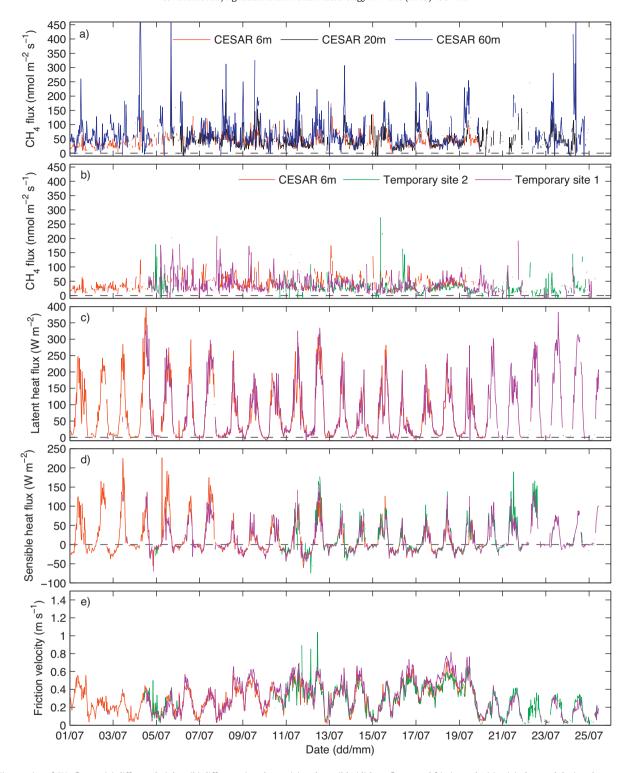
Fig. 3. Time series of CH_4 fluxes: (a) different heights, (b) different sites, latent (c) and sensible (d) heat fluxes and friction velocities (e) observed during the campaign. The CH_4 flux is plotted only for periods when flux stationarity (Foken and Wichura, 1996) were below 0.3.

statistical test, the differences between the sites were significant (null hypothesis can be rejected at $p < 0.001$ level).

In general the CH_4 fluxes were higher and more variable at the 60 m level than at the lower measurement levels (Fig. 3a). Especially in wind direction 250–280° marked differences between F_{CH_4} from different heights were observed (compare Fig. 4b, d and f). This is most likely related to the CH_4 emissions originating from the nearby farms, which were captured by the 60 m level flux system and partly also with the 20 m level system, but not with the

6 m flux system. These farm CH_4 emissions are discussed further in Section 3.6, whereas the other sections concentrate on CH_4 fluxes originating from the soil only. Farm emissions were removed by discarding records when farms were within the footprint (inside 90th percentile) or when wind direction at the CESAR site was from the 250 to 280° sector. A median value of 47 nmol m^{-2} s^{-1} was obtained for the 60 m level CH_4 fluxes and 37 nmol m^{-2} s^{-1} for the 20 m level CH_4 fluxes after removing the periods affected by farm emissions.
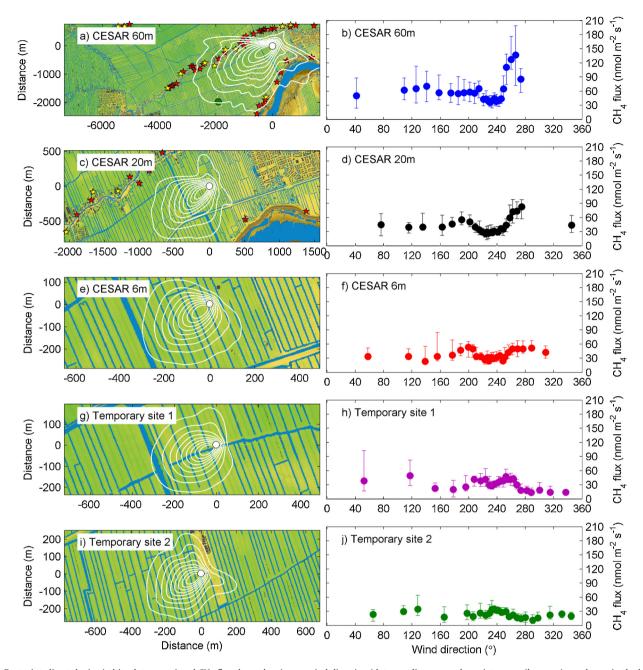
Fig. 4. Footprint climatologies (white dot: tower) and CH_4 flux dependencies on wind direction (dots: medians; error bars: interquartile range) are shown in the left and right columns, respectively. The contours in the footprint climatology plots are plotted with 10 percentile intervals; the outermost contours show 90th percentiles and the innermost show 10th percentiles. The yellow and red stars in panels (a) and (c) represent the location of farms (For interpretation of the references to colour in this figure legend, the reader is referred to the web version of this article.).

Of the three short tower sites, a statistically significant diel pattern in the F_{CH_4} time series was only seen at the CESAR 6 m site ($p < 0.01$, Wilcoxon rank sum test to test whether the night time and daytime CH_4 fluxes came from the same distribution. Autocorrelation between the data points was taken into account with the variance inflation factor). The daytime (incoming short wave radiation >5 W m^{-2}) fluxes were 9 nmol m^{-2} s^{-1} (difference between medians) larger than night time (incoming short wave radiation <5 W m^{-2}) fluxes (Fig. 5c). However, the diel pattern was evident only in certain wind direction (roughly 160° to 250°), not in other directions (not shown). At the other short tower sites the differences between day and night were negligible. Interestingly, the difference between the CESAR 6 m site and the two other tower sites was smaller at night (approximately 1 and 4 nmol m^{-2} s^{-1}

compared to Temporary site 1 and 2, respectively) than at day (9 and 16 nmol m^{-2} s^{-1}, respectively).

In addition to the 6 m level, a statistically significant diel pattern was observed in CH_4 flux at the 20 m height ($p < 0.001$, Wilcoxon rank sum test), but not at 60 m height ($p > 0.05$). The amplitude of the diel pattern was 11 nmol m^{-2} s^{-1} at 20 level, daytime fluxes being larger than night time (Fig. 5d).

3.4. Partitioning the variance observed between the three short towers

3.4.1. Variances calculated using 30-min averaged fluxes

The landscape CH_4 flux variance, i.e. the total variance, was calculated from the data obtained with the three short towers and
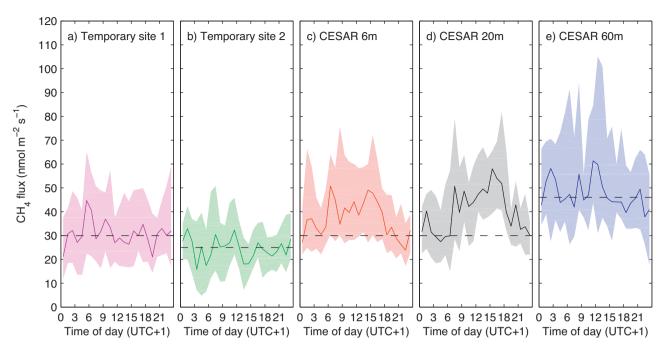
Fig. 5. Diel variations of CH_4 fluxes (line: median, area: interquartile range). Only periods when farms were outside the footprint were used. Dashed lines show typical night time values.

divided into three components with Eq. (3). This was done in order to assess the relative importance of spatial and temporal variability, in addition to instrument related variance, on landscape level flux variability. The tested CH_4 flux instruments agreed within 7% (CV_{ins} = 0.07, variability between mean fluxes from the six different instruments) in the Peltola et al. (2014) intercomparison study, during which the instruments were measuring at the same location almost one month. This result was used to estimate σ^2_{ins} and used in partitioning the total CH_4 flux variance with Eq. (3) in this study. The total coefficient of variation (CV_{tot}) was 0.71, the spatial CV (CV_{spa}) was 0.56 and the temporal CV (CV_{tem}) was 0.43 for CH_4 fluxes during the campaign. The spatial, temporal and instrument related variance terms contributed 62%, 37% and 1% to the total variance, respectively.

In order to put this result into context the landscape scale variance of sensible heat flux (H) and friction velocity (u_*) were also divided into three components. For H only periods when $|H| > 20\,W\,m^{-2}$ were used in order to get meaningful values for CV (Katul et al., 1999). Again, results from the Peltola et al. (2014) intercomparison study were used to estimate the instrument related variance for H and u_* (H: CV_{ins} = 0.04, u_*: CV_{ins} = 0.02, variability between mean fluxes). For those variables the spatial terms were 9% and 8% of the total variance (H: CV_{spa} = 0.26, u_*: CV_{spa} = 0.13), the temporal terms were 91% and 92% of the total variance (H: CV_{tem} = 0.83, u_*: CV_{tem} = 0.45) and the instrument related variances were less than 1% of the total variance for both parameters. Thus, for those variables the total variance was dominated by the temporal variability term, unlike the total variance of CH_4 flux which was governed by the spatial variability term. This can be interpreted in such a way that measurements at a single tower represent the whole landscape better for sensible heat fluxes and friction velocities than for the CH_4 flux. A similar result was found for CO_2 flux (F_{CO_2}) by Katul et al. (1999): in their study the spatial variability was ranked $F_{CO_2} > H > u_*$. These results can also qualitatively be observed in the flux time series plotted in Fig. 3.

As discussed by Oren et al. (2006) and Katul et al. (1999) the variances calculated using 30-min flux values are largely affected by the sampling errors of the fluxes. In Oren et al. (2006) the spatial

variance decreased when the flux data were averaged in time (random variability was averaged out) and a stable minimum for CV_{spa} was acquired after a few hours of averaging. Thus the variance values reported above cannot be used to describe the persistent spatial variation, which is caused only by the source/sink variability in the area, since the values above are hampered by the sampling errors. However, the values above do describe how well EC CH_4 measurements at one short tower represent the landscape CH_4 flux (area between the three short towers) on the 30-min time scale. The magnitude of the persistent spatial variation which characterises better the landscape level long term spatial variability is discussed in the next section.

3.4.2. Variability between temporally averaged CH_4 emissions

The F_{CH_4} time series from the three short towers were averaged over 24 h in order to study the relative significance of temporal and spatial variability between sites at the daily scale. The inter-day CV_{spa} was 0.22 and CV_{tem} was 0.19. Spatial variability contributed 52% and temporal variability 41% to the total landscape scale variance. Thus the relative importance of spatial variability decreased when compared to the 30-min averaged flux case (Section 3.4.1), however the spatial and temporal terms in Eq. (3) were still of similar magnitude.

In order to evaluate the effect of temporal averaging on spatial variability estimate CV_{spa}, the flux time series were averaged in time with a varying averaging window and then the variances were estimated. The results are shown in Fig. 6. Similarly to Oren et al. (2006) at first CV_{spa} decreased rapidly when averaging time was increased, but after a certain threshold value was reached, CV_{spa} remained practically constant (CH_4 flux: 0.14–0.17, H: 0.06–0.08, u_*: 0.05–0.07). This corresponds to averaging out the site internal variability after which the CV_{spa} describes only to the persistent spatial variance. It is an intrinsic property of the landscape and it describes the heterogeneity of the fluxes at a horizontal scale of a few kilometres, i.e. the distances between the three short towers. CV_{spa} decreased since the random uncertainty was averaged out, however the decrease was significantly smaller than expected from
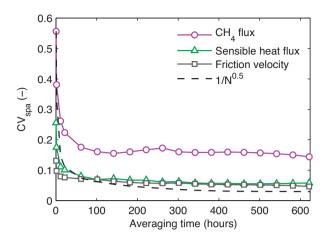
Fig. 6. The dependency of CV_{spa} on flux averaging time. The dashed black line shows the decrease if the spatial variability in CH_4 flux CV_{spa} would be related only to a random process.

Fig. 7. The difference between CH_4 fluxes at 6 m height and upper heights (a) and the coefficient of variation between the three heights ($CV_{6,20,60}$) (b). The instrument related variance (σ^2_{ins}) was removed from $\sigma^2_{6,20,60}$ before calculating $CV_{6,20,60}$. The lines show the medians and the areas show the interquartile ranges around the medians. The dashed line in the upper plot highlights the zero line.

purely random fluctuations (compare the black dashed line and the purple line with circles in Fig. 5).

CV_{spa} was 0.14 for long term means of CH_4 flux. It contributed 80% to the total variance (σ^2_{tot}) observed between the mean CH_4 fluxes at the three short tower sites, whereas instrument related variance (σ^2_{ins}) contributed the remaining 20%. The total coefficient of variation (CV_{tot}) was 0.16. The value of CV_{spa} is specific to the landscape and most likely also slightly to the time of year, since CH_4 flux at different parts of the landscape may respond in diverse ways to seasonal changes in different environmental drivers. Furthermore, CV_{spa} presumably varies between scalar fluxes (for instance CO_2, CH_4, N_2O fluxes), since they depend on different driving variables which exhibit different degree of spatial variability.

3.4.3. Assessing the significance of spatial variability on annual scale

In order to study the significance of the estimated spatial variance on annual scale, the results shown in Section 3.4.2 were combined with annual emissions estimates published earlier by Kroon et al. (2010). Using methods described in Appendix B the importance of spatial and instrument related variance on the annual scale was estimated, in addition to the gap filling uncertainty which was obtained from the original paper. The uncertainty related to gapfilling was the dominant component of the total uncertainty, contributing between 83% (year 2008) and 97% (2007) to the total annual uncertainty (Table 4). The spatial variability term added between 2% (2007) and 13% (2008) to the total uncertainty and the instrument related term was only a few percent of the total uncertainty. However, the annual data coverage of the Oukoop measurements was relatively low (between 29% and 52%) and thus it is understandable that the gap filling was the biggest source of uncertainty because the annual sums were comprised mostly from gap filled data. If the calculations were done by assuming a data coverage of 75%, which is a typical value for EC sites, the relative contribution of gapfilling would decrease (38%), whereas the contribution of spatial variability and instrument related uncertainty to estimating fluxes at the landscape scale would increase (to 49% and 12%, respectively).

3.5. Comparison of tall tower and short tower CH_4 fluxes

3.5.1. Comparison with the three short towers

The variability between the F_{CH_4} at different heights, measured as the coefficient of variation between the three EC flux measurement levels ($CV_{6,20,60}$; 60 m and 20 m levels at the CESAR site and
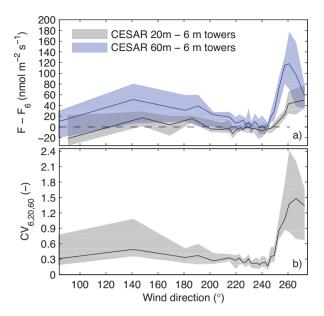
three locations at 6 m height), was on average 0.25 (no farms in the footprint). $CV_{6,20,60}$ was smallest (approximately 0.18) in the direction (230–240°) where the fetch of fields and drainage ditches at the CESAR site was least disturbed (see Figs. 4 and 7). Especially the fluxes at 60 m level deviated from the 6 m fluxes (median absolute and relative difference were 7 nmol m^{-2} s^{-1} and 21%, respectively, when there were no farms in the footprint), the difference between fluxes at 20 m and 6 m levels was smaller (−4 nmol m^{-2} s^{-1}, 12%).

According to the blending height concept (e.g. Mahrt, 2000) and footprint modelling (Rannik et al., 2012) the tall tower fluxes should represent the landscape fluxes better when wind speed or atmospheric stability is increased or BLH is decreased. This is due to the fact that the size of the footprint is increased and thus fluxes from a larger area were aggregated. The relative difference between fluxes measured at the two levels ((F(60 m) − mean(F(6 m))/mean(F(6 m)) did not decrease with increasing stability parameter ζ (unstable ($\zeta < -0.1$): 0.09, near neutral ($|\zeta| < 0.1$): 0.10, stable ($\zeta > 0.1$): 0.26) or decreasing mixed layer height (high ($h > 482$ m): 0.18, moderate (285 m $< h < 482$ m): 0.32, low ($h < 285$ m): 0.12). However, a small dependence on wind speed U (low ($U < 4.2$ m s^{-1}): 0.36, moderate (4.2 m s^{-1} $< U < 6.1$ m s^{-1}): 0.15, high ($U > 6.1$ m s^{-1}): 0.07) was observed, although the (anti-)correlation between U and the flux difference was negligible (−0.17, Spearman's rho). Also it should be kept in mind that during low wind speed and/or highly stable conditions EC flux measurements tend to have significant problems since turbulent mixing is intermittent and weak and thus the measured flux does not necessarily relate to the flux at the surface. Furthermore, periods with significant changes in the boundary layer mixing may cause discrepancies between fluxes at different levels (see the next section).

3.5.2. Vertical variability of CH_4 fluxes during morning and evening transition periods

During some days the CH_4 fluxes at different heights showed marked differences when the transition between stably stratified night time and unstable daytime boundary layer took place. Due to the relatively short duration of the study it is not possible to make a comprehensive quantitative analysis of these transition periods,

Table 4
Annual CH_4 emissions (g(CH_4) m^{-2} yr^{-1}) at Oukoop site (Kroon et al., 2010). Values in parentheses show the relative contribution of each uncertainty component to the total uncertainty based on the results in Section 3.4.3.

	CH_4 emission	Data coverage (%)	Uncertainty components			
			Gap-filling	Instrument	Spatial variability	Total
2006	17.6	33	4.4 (96)	0.4 (1)	0.8 (3)	4.5
2007	16.9	29	4.4 (97)	0.3 (1)	0.7 (2)	4.5
2008	14.9	52	2.7 (83)	0.5 (3)	1.1 (13)	2.9
Simulation[a]	16.5	75	1.5 (38)	0.9 (12)	1.7 (49)	2.5

[a] Estimation of the uncertainty components in a case when the annual data coverage is 75%. Mean annual CH_4 emission at the site (16.5 g(CH_4) m^{-2} yr^{-1}) was used in this case.

instead examples from two days (4.7.2012 and 23.7.2012) when the wind was not blowing from the farms are shown.

The night prior to 4.7.2012 was moderately stable ($z_m/L = 0.4$), although windy (wind speed = 2.1 m s^{-1}), which resulted in a strong vertical gradient in CH_4 dry mixing ratio within the nocturnal boundary layer (−4 ppb m^{-1}). After the onset of convective mixing in the morning of 4th of July (06:00 local time) the turbulent CH_4 flux at 60 m height showed a large positive peak (695 nmol m^{-2} s^{-1}). The peak was partly dampened by adding the storage change term (compare blue dashed and solid lines in Fig. 8c), but still a clear difference between 6 m and 60 m heights remained (475 nmol m^{-2} s^{-1}). However, later during the same morning (07:30–10:30) the difference was largely explained by the storage change term: it reduced from 128 nmol m^{-2} s^{-1} to

31 nmol m^{-2} s^{-1} after adding the term, respectively. If it is assumed that the fluxes should be the same during the morning period as later during the same day, it is possible to estimate how big fraction of the estimated flux was purely due to the changes in boundary layer mixing in the morning, i.e. not related to surface flux. Median differences between midday (11:00–15:00) and the morning period (05:30–10:30) CH_4 fluxes were 92 nmol m^{-2} s^{-1} (72% relative difference) and 16 nmol m^{-2} s^{-1} (42%) for 60 m and 6 m fluxes, respectively. Regarding the evening transition, the CH_4 fluxes at 6 m height showed a spurious spike when the convective boundary layer collapsed (Fig. 8a and c).

Qualitatively similar behaviour was observed in 23.7.2012 (Fig. 8b and d). The conditions during the previous night ($z_m/L = 1.1$, wind speed = 2.0 m s^{-1}, CH_4 gradient = −4 ppb m^{-1}) were
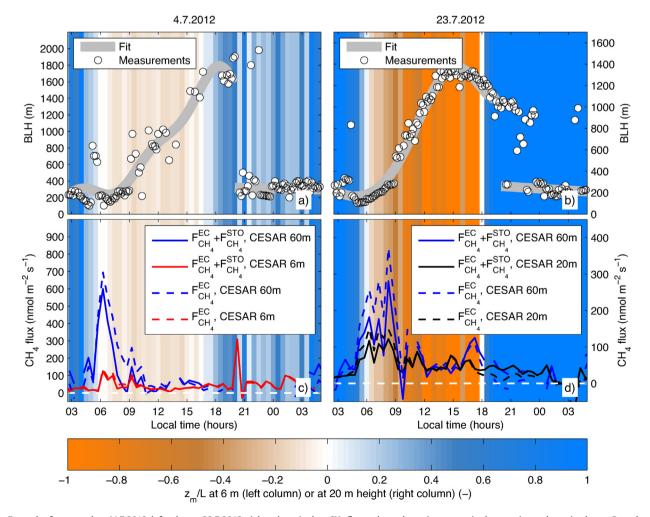

Fig. 8. Examples from two days (4.7.2012, left column; 23.7.2012, right column) when CH_4 fluxes showed erratic patterns in the morning and evening hours. Boundary layer heights (BLH) are in the top row and CH_4 fluxes (with and without the storage change term, $F_{CH_4}^{STO}$) in the bottom row. Note change in scale in y-axes.
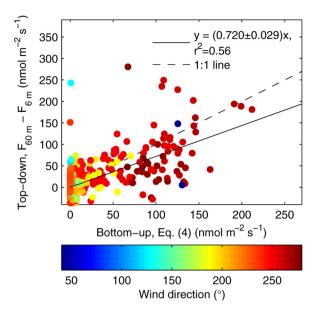
Fig. 9. Scatter plot of bottom-up and top-down estimates for the farm CH_4 emissions. Colours of the points denote wind direction (For interpretation of the references to colour in this figure legend, the reader is referred to the web version of this article.).

comparable with the night prior to 4.7.2012. During the morning transition period after adding the storage change term the differences between 60 m and 20 m height fluxes were not negligible (median: 42 nmol m^{-2} s^{-1}) and they both deviated from their corresponding daytime fluxes: 81 nmol m^{-2} s^{-1} (66%) and 37 nmol m^{-2} s^{-1} (46%) deviation in 60 m and 20 m fluxes, respectively. During the evening period when the convective boundary layer collapsed, the $F_{CH_4}^{EC}$ at 60 m height was occasionally negative, however after adding the storage change term the flux changed sign and was comparable with 20 m height flux (see Fig. 8b and d time period 20:00–21:00). These two days exemplify the fact that the boundary layer mixing conditions have larger impact on fluxes high above the ground than closer to the surface.

3.6. Estimating CH_4 emissions from farms using top-down and bottom-up methods

Figs. 9 and 10 show comparisons between two independent estimates for the farm emissions: (1) the BUE calculated based on

the CH_4 emission factors and the 60 m level footprint (Eq. (4)) and (2) the TDE, namely the difference between F_{CH_4} at 60 m and 6 m levels. Similar analysis was not possible with 20 m and 6 m level fluxes since the 20 m level footprint did not encompass the farms as clearly as the 60 m level footprints (compare Fig. 4a and c). The BUE explains 56% of the variation seen in the TDE (difference between 60 m and 6 m level fluxes) and the linear fit to the two estimates had a slope of 0.720 ± 0.029 (Fig. 9). BUE was thus on average 28% larger than TDE. If the assumptions underpinning TDE are correct, this could suggest that CH_4 emissions per animal at the studied landscape were on average 28% smaller than reported by Coenen et al. (2014). Thus the agreement is relatively good, given the uncertainty of the EF estimates (Table 1), the fact that manure emissions were neglected and that the TDE is not applicable during periods when BLH is below 60 m (although such periods were not observed). In addition, animals may have been out grazing at times and emission factors may vary over the year, while the measurements here can only present a snapshot in time. In any case, as a first order estimate, the TDE should be valid.

The agreement between BUE and TDE depended on wind direction: for wind directions in the 240–260° sector the slope was 0.844 ± 0.045 compared to 0.618 ± 0.074 in the 260–280° sector (see also Fig. 10). Thus, the BUE overestimated the farm CH_4 emissions especially in wind direction 260–280° (38% overestimation), whereas in wind direction 240–260° the difference was smaller (16% overestimation). In the latter wind direction range, emissions factors (Table 1) characterised farms reasonably well.

4. Discussion

In this study the spatial variability of CH_4 fluxes were estimated with three short towers, in addition to two taller towers. An estimate for the spatial variation of F_{CH_4} was given at 30-min ($CV_{spa} = 0.56$) and long-term scale ($CV_{spa} = 0.14$) in Section 3.4. The difference between these two values can be assumed to characterise the CH_4 flux variability at 30-min scale caused by site internal CH_4 flux spatial variability, meaning the stochastic nature of turbulence and variability of the CH_4 flux when wind direction and speed (i.e. footprint) change at each site, in addition to different short term flux patterns at each site (diel cycle vs. no diel cycle, ebullition). Although substantial, the spatial variability reported in this study was significantly smaller than what was reported earlier in a chamber study by Hendriks et al. (2010). They estimated CH_4 emissions at a similar ecosystem as this study with several chambers and found up to 25-fold differences ($CV_{spa} = 1.03$) between the chamber plots. Thus the CH_4 flux spatial variability is an order of
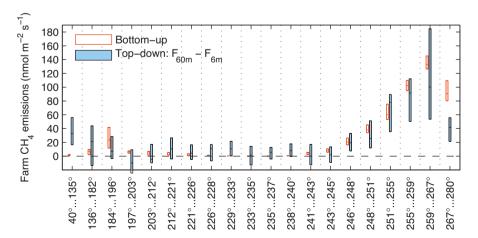

Fig. 10. Comparison between the bottom-up and top-down estimates for the farm CH_4 emissions in different wind directions at the CESAR site. The boxes denote the interquartile ranges and the lines within the boxes show the medians. Note that the wind direction bins vary in width.

magnitude higher at the plot scale (∼1 m², chambers) than at the ecosystem scale (∼1 ha, short tower EC). In order to estimate the landscape scale fluxes from chamber measurements, the differing proportions of different field and landscape features (for instance hummocks, hollows, ditches) need to be taken into account and the chamber measurements are upscaled based on these proportions (e.g. Hendriks et al., 2010; Schrier-Uijl et al., 2010b; Teh et al., 2011). This is an error-prone exercise and also detailed information about the landscape elements is needed. Therefore EC fluxes are generally better suited for upscaling to landscape scale.

Temporal variability and spatial variability between the three short tower sites were of similar magnitude on a daily scale (CV_{spa} = 0.22, CV_{tem} = 0.19). This has important implications for instance for CH_4 flux modelling, since it is often done with daily time step (Zhu et al., 2014). If the landscape scale fluxes are to be modelled accurately then it is as important to model the temporal variability exactly as it is to capture the spatial variance on few kilometre scales.

The spatially variable CH_4 fluxes observed with the three short towers (differences in mean fluxes and diel patterns) indicated that there were either differences in (1) CH_4 production, (2) oxidation of CH_4 or (3) transport (via diffusion, ebullition or plant aerenchyma). At the CESAR site the water level at the ditches was closer to the surface than at the other sites and thus likely a smaller fraction of the produced CH_4 was oxidised while it diffused through the aerobic soil layer to the atmosphere. Furthermore, certain methane-conducting plants which thrive in very moist soils (such as *J. effusus*) were observed at the site. These can decrease the amount of oxidised CH_4 since they provided a quick bypass route past the oxic soil layer (Henneberg et al., 2012). In addition to water level, Hendriks et al. (2010) and Lai et al. (2014) found rooting depth to be an important explaining variable for the spatial variability of CH_4 fluxes. Plant roots add labile carbon to soil which can be used for bacterial methanogenesis (e.g. Chanton et al., 1995; Whiting and Chanton, 1993), in addition to being a major pathway for CH_4 to the atmosphere in aerenchymatous plant species. Diel variations in the CH_4 flux are often linked to plant-mediated CH_4 transport, specifically in plants with convective through-flow through the aerenchyma (Hendriks et al., 2010; Kim et al., 1999; Matthes et al., 2014). However, no plants with this transport mechanism were identified at the CESAR site where the strongest diel pattern in CH_4 flux was observed. In any case, the fact that a diel pattern was observed at one site and at others not, in addition to different mean CH_4 flux levels, suggests that there were different controls on CH_4 emissions at different sites and the related spatial variability should be taken into account if defensible landscape scale CH_4 emissions are to be estimated.

On average, F_{CH_4} was higher at 60 m level than at lower levels indicating that a distant source of CH_4 (in addition to the farms) was observed with the tall tower and not with the short towers. Some of the deviations could be explained with the farm emissions (Section 3.6) and spurious fluxes during the morning and evening transition periods (Section 3.5.2). Entrainment flux at the top of the BLH may influence the vertical variability of turbulent fluxes, especially when the boundary layer starts growing in the morning. For instance Casso-Torralba et al. (2008) and de Arellano et al. (2004) found that the entrainment flux of CO_2 was about three to five times larger than the surface flux during morning hours. Evidently, in such situation the turbulent fluxes high above the ground do not represent the surface fluxes accurately. CH_4 flux vertical variability seen during the two mornings in this study (Section 3.5.2) might be partly related to entrainment, since it amplifies the upward directed turbulent CH_4 flux by bringing air with low CH_4 mixing ratio from the free atmosphere to the upper parts of the boundary layer. However, it should be emphasised that the sum of the

vertical turbulent flux and the storage change term should be constant with height and equal the surface flux, regardless of entrainment. Nevertheless, this requires that the measurements describe these two terms accurately so that any effects of entrainment on the vertical turbulent flux are balanced by similar (but opposite sign) changes in the storage change term. Furthermore, also the other terms in mass balance equation (i.e. advection and horizontal turbulent flux divergence) may complicate the situation during these transition periods. Thus it can be concluded that the disadvantage of conducting EC measurements high above the surface is that then the turbulent fluxes are not as directly linked with the surface fluxes as EC measurements at lower levels.

The multilevel (6 m, 20 m and 60 m) EC CH_4 measurements at the CESAR site allowed the high CH_4 emissions from the farms to be located and quantified. Detailed source area modelling with a state-of-the-art footprint model (Kljun et al., 2004) was essential in understanding the differences in CH_4 fluxes at different measurement levels. This result highlights the significance of footprint modelling when interpreting EC measurements and on the other hand suggests that the used model is applicable in assessing tall tower fluxes' source areas. In general, multilevel flux systems and concurrent footprint modelling can be used to locate strong point sources and to study the flux spatial variability which is useful if the flux in question shows high horizontal variability, like CH_4 often does. This approach may also be useful to identify and quantify unknown vents from landfill, disused mines and/or fracking.

Most of the variability (80%) between the short tower site long term means was caused by spatial variability of CH_4 surface flux and only 20% could be attributed to differences between instrumentation and data processing schemes. As presented by Peltola et al. (2014) and also by (Detto et al., 2011; Iwata et al., 2014; Peltola et al., 2013) the overall agreement between commonly used EC CH_4 analysers is good and data processing schemes are relatively well-developed. Thus it can be argued that the variability observed between the sites was real and not caused by instrumental differences, and further that the usability of one short tower in estimating landscape scale CH_4 fluxes cannot be enhanced significantly by instrument development or improvement of data processing routines. Furthermore, at the annual scale the most important sources of uncertainty were related to flux spatial variability and gapfilling, and the instrument related uncertainty was found to be of minor importance.

5. Summary and conclusions

Three short towers (6 m) and two EC systems at higher levels (20 m and 60 m) were used to study the spatial variability of CH_4 emissions, spatial representativeness of one short EC tower and applicability of the tall tower measurements in estimating landscape scale CH_4 fluxes. The measurements were conducted at an agricultural temperate peatland landscape which is a significant source of CH_4 to the atmosphere.

Considerable differences between the three short towers were observed, and also deviating diel patterns suggest differences in CH_4 production, oxidation and/or transport paths to the atmosphere. The coefficient of variation between the mean emissions from three short towers was 0.16 and 80% of this variability was caused by CH_4 flux spatial variability. The tall tower system observed emissions from sources which were not detected by the three short towers and thus provided a different view on the large scale CH_4 emissions at the studied landscape. The mean estimated tall tower CH_4 emission was however reasonably close (21% relative difference) to the mean observed at the three short towers.

Higher CH$_4$ fluxes were observed at the 60 m height than at the two lower measurement heights at the CESAR site, especially for certain wind directions. These differences were related to CH$_4$ emissions originating from nearby dairy farms, which were confirmed by footprint, i.e. source area, modelling and bottom-up CH$_4$ flux estimation based on emission factors. This result highlights the usability of multilevel EC measurement system in locating and quantifying strong point sources in the landscape.

Finally, the differences observed between the three short tower sites emphasise the need for CH$_4$ flux data with larger spatial integration if landscape scale exchange is of interest. At the annual scale, up to 49% of the flux uncertainty was caused by spatial variability which illustrates the fact that the regular EC short tower does not average fluxes over large enough area to provide an accurate estimate of the whole landscape scale exchange. More spatial integration could be achieved with aeroplane EC measurements (e.g. Hiller et al., 2014), nocturnal boundary layer method (e.g. Pattey et al., 2002), tall tower EC measurements accompanied with concentration profiles for storage change calculations (e.g. Desai et al., 2015; Winderlich et al., 2014) or with high resolution CH$_4$ flux modelling (e.g. Zhu et al., 2014). Out of these alternatives, despite their shortcomings tall tower EC systems are the most attractive option due their ability to measure CH$_4$ exchange directly with high temporal resolution, continuously over extended periods of time.

Acknowledgements

Appendix A. EC data processing and screening

The following procedure was applied when EC data was processed:

1. The high frequency CH$_4$ data were despiked by comparing two adjacent data points, if their difference was larger than 3 ppm the following point was replaced with the same value as in the previous point. Despiking may bias the fluxes low when many consecutive points are considered as spikes.
2. After despiking, the effect of H$_2$O on the measured CH$_4$ (density and spectroscopic effects) was corrected point-by-point in those CH$_4$ time series which were measured simultaneously for H$_2$O with the same analyser.
3. The angle of attack correction based on Nakai and Shimoyama (2012) was applied to data measured with Gill anemometers.
4. The coordinate system was rotated with the 2D-coordinate rotation method: in which the anemometer coordinates were aligned with the mean wind and further the mean vertical wind component during the 30-min averaging period was zero ($\bar{w} = 0$).
5. In the next step, the time lag between the vertical wind velocity and gas measurements, which was induced by the sampling system, was estimated by searching the maximum deviation of the crosscovariance function from zero in a predefined window and then the covariance was calculated using the estimated lag.
6. For those analysers without an internal H$_2$O measurement, CH$_4$ fluxes were corrected for H$_2$O effects (Peltola et al., 2014).
7. All the fluxes were corrected for bandpass filtering induced by the sampling system and data processing. The response times used in correcting the fluxes for low-pass filtering with a transfer function described by Horst (1997) are given in Table 2. The transfer function describing high-pass filtering was acquired from Rannik and Vesala (1999).

Flux data were screened in order to remove erroneous measurements prior to analysis. The following criteria were used to identify and remove unphysical and/or unusual CH$_4$ flux data:

- More than 3000 spikes were found during an averaging period (see Point 1 in the previous list for spike detection).
- The CH$_4$ flux was unrealistic for this site (outside the range -50 to 2000 nmol m^{-2} s^{-1}).
- 30-min mean concentration was unrealistic (outside the range 1.7–3.5 ppm).
- Sonic anemometer data were unrealistic (evaluated based on skewness and kurtosis of wind components and sonic temperature or the value for the second coordinate rotation angle).
- The flux stationarity test (Foken and Wichura, 1996) yielded larger value than 1.

Furthermore, fluxes measured at CESAR 20 m and 60 m were removed when the wind was blowing from the 280 to 340° sector, since then the measurement system was in the wake of the tower and thus the measured turbulent fluxes were unreliable due to the structural influence of the tower on the turbulence regime. No screening based on wind direction was done for the other measurement locations since the tower constructions were light (Fig. 1). Also, data were not filtered based on friction velocity, since no clear friction velocity threshold was found at any of the flux EC measurement locations. After this screening procedure a data coverage of 73%, 55%, 73%, 63% and 47% was maintained for CESAR 60 m, CESAR 20 m, CESAR 6 m, Temporary site 1 and Temporary site 2, respectively.

Since many of the fields in the area were used as a pasture, and grazing ruminants were occasionally seen, especially in the vicinity of Temporary site 1, the effect of CH$_4$ emissions from the grazing cattle needed to be estimated. It was assumed that animals moving in and out of the flux footprint added short term positive peaks to the measured CH$_4$ time series. These short term peaks were identified by calculating the skewness of the high frequency CH$_4$ time series for each 30-min averaging period. Periods with skewness larger than 3.5 were excluded from further analysis. This threshold was empirically determined based on CH$_4$ measurements at the Temporary site 1. Large positive values for skewness indicate that the data are skewed towards significant positive deviations from the mean. Vickers and Mahrt (1997) used skewness to detect faulty data, but in this study it is used to remove unwanted measurements. In total of 4.5% (54 points), 1.4% (17) and 0.5% (6) of the CH$_4$ flux data were flagged as being possibly affected by the animals for Temporary site 1, Temporary site 2 and CESAR 6 m, respectively. This agrees with visual observations during the campaign: cows were mostly seen in the vicinity of Temporary site 1.

Appendix B. Uncertainty on annual scale

In Kroon et al. (2010), the annual CH_4 emission (F_{ann}) was calculated by summing the measured and gapfilled data

$$F_{ann} = \sum_{i=1}^{N_m} F_m^i + \sum_{j=1}^{N_g} F_g^j, \tag{B.1}$$

where N_m and N_g were the amount of measured and gapfilled data, respectively, and F_m and F_g were the flux time series obtained with EC and gapfilling. The error variance of F_{ann} was calculated using propagation of error of uncorrelated variables

$$\Delta(F_{ann})^2 = \Delta\left(\sum_{i=1}^{N_m} F_m^i\right)^2 + \Delta\left(\sum_{j=1}^{N_g} F_g^j\right)^2. \tag{B.2}$$

The first term on the right side (error variance of the sum of the F_m time series) was estimated using the relative uncertainty related to the spatial variability of the long-term means ($u_{spa} = 0.14$) and instrument related uncertainty ($u_{ins} = 0.07$), whereas the second term (error variance of the sum of the gapfilled fluxes) was estimated using relative uncertainty of the gapfilling method ($u_{gap} = 0.37$), which was acquired from Kroon et al. (2010). Thus

$$\Delta(F_{ann})^2 = \left(u_{spa}\sum_{i=1}^{N_m} F_m^i\right)^2 + \left(u_{ins}\sum_{i=1}^{N_m} F_m^i\right)^2 + \left(u_{gap}\sum_{i=1}^{N_g} F_g^i\right)^2. \tag{B.3}$$

Next it was approximated that the gapfilled fluxes and the fluxes obtained with EC have the same mean and thus by definition

$$\Delta(F_{ann})^2 \approx \left(u_{spa}\frac{N_m}{N}F_{ann}\right)^2 + \left(u_{ins}\frac{N_m}{N}F_{ann}\right)^2 + \left(u_{gap}\frac{N_g}{N}F_{ann}\right)^2, \tag{B.4}$$

where $N = N_m + N_g$. When estimating the annual uncertainty, the yearly data coverage (N_m/N) and emission (F_{ann}) were acquired from Kroon et al. (2010) and they are also given in Table 4.

Appendix C. Footprint calculations

Footprints were calculated for each EC measurement location in order to assess its size and identify the sources affecting the measurements. The turbulent flux at height z_m, $F(0,0,z_m)$, is related to the flux field at the surface ($f(x,y,0)$) via the footprint function $\phi(x, y, z_m)$:

$$F(0, 0, z_m) = \iint f(x, y, 0)\phi(x, y, z_m)dxdy. \tag{C.1}$$

The footprint function ϕ gives the relative contribution of each point in the $(x,y,0)$ plane to the turbulent flux (Rannik et al., 2012). In other words, the flux, F, can be considered as a weighted average of the flux at the surface, where the footprint function acts as a weighting function. In this study a parameterisation (Kljun et al., 2004) of a three-dimensional backward Lagrangian footprint model (Kljun et al., 2002) was used.

A footprint was calculated for each 30-min flux value and overlaid on a grid (resolution 3 m) in the prevailing wind direction and thus the contribution of each grid cell to the EC CH_4 flux could thus be assessed. The footprint climatology at each EC measurement location was estimated by summing up all the footprints which were overlaid on this common grid.

References

Beljaars, A.C.M., Bosveld, F.C., 1997. Cabauw data for the validation of land surface parameterization schemes. J. Clim. 10 (6), 1172–1193.

Casso-Torralba, P., et al., 2008. Diurnal and vertical variability of the sensible heat and carbon dioxide budgets in the atmospheric surface layer. J. Geophys. Res. Atmos. 113 (D12), D12119.

Chanton, J.P., et al., 1995. Radiocarbon evidence for the substrates supporting methane formation within northern Minnesota peatlands. Geochim. Cosmochim. Acta 59 (17), 3663–3668.

Coenen, P.W.H.G., et al., 2014. Greenhouse Gas Emissions in The Netherlands 1990–2012 National Inventory Report 2014. National Institute for Public Health and the Environment, Bilthoven.

de Arellano, J.V.-G., et al., 2004. Entrainment process of carbon dioxide in the atmospheric boundary layer. J. Geophys. Res. Atmos. 109 (D18), n/a-n/a.

De Haij, M.J., Wauben, W.M.F., Klein Baltink, H., 2007. Continuous Mixing Layer Height Determination Using the LD-40 Ceilometer: A Feasibility Study. WR-2007-01, KNMI, De Bilt.

Desai, A.R., et al., 2015. Landscape-level terrestrial methane flux observed from a very tall tower. Agric. For. Meteorol. 201 (0), 61–75.

Detto, M., Verfaillie, J., Anderson, F., Xu, L., Baldocchi, D., 2011. Comparing laser-based open- and closed-path gas analyzers to measure methane fluxes using the eddy covariance method. Agric. For. Meteorol. 151 (10), 1312–1324.

Foken, T., Aubinet, M., Leuning, R., 2012. The eddy covariance method. In: Aubinet, M., Vesala, T., Papale, D. (Eds.), Eddy Covariance. Springer Atmospheric Sciences, Springer Netherlands, pp. 1–19.

Foken, T., Wichura, B., 1996. Tools for quality assessment of surface-based flux measurements. Agric. For. Meteorol. 78 (1–2), 83–105.

Hendriks, D.M.D., van Huissteden, J., Dolman, A.J., 2010. Multi-technique assessment of spatial and temporal variability of methane fluxes in a peat meadow. Agric. For. Meteorol. 150 (6), 757–774.

Henneberg, A., Sorrell, B.K., Brix, H., 2012. Internal methane transport through Juncus effusus: experimental manipulation of morphological barriers to test above- and below-ground diffusion limitation. New Phytol. 196 (3), 799–806.

Hiller, R.V., et al., 2014. Aircraft-based CH4 flux estimates for validation of emissions from an agriculturally dominated area in Switzerland. J. Geophys. Res. Atmos. 119 (8), 4874–4887.

Horst, T.W., 1997. A simple formula for attenuation of eddy fluxes measured with first-order-response scalar sensors. Bound. Layer Meteorol. 82 (2), 219–233.

Iwata, H., et al., 2014. Cross-validation of open-path and closed-path eddy-covariance techniques for observing methane fluxes. Bound. Layer Meteorol. 151 (1), 95–118.

Jager, C.J., Nakken, T.C., Palland, C.L., 1976. Bodemkundig onderzoek van twee graslandpercelen nabij Cabauw. NV Heidemaatschappij Beheer, Arnhem (available by request at http://www.knhm.nl).

Joosten, H., Clarke, D., 2002. Wise Use of Mires and Peatlands: Background and Principles Including a Framework for Decision-making. International Mire Conservation Group and International Peat Society, pp. 304.

Katul, G., et al., 1999. Spatial variability of turbulent fluxes in the roughness sublayer of an even-aged pine forest. Bound. Layer Meteor. 93 (1), 1–28.

Kim, J., Verma, S.B., Billesbach, D.P., 1999. Seasonal variation in methane emission from a temperate Phragmites-dominated marsh: effect of growth stage and plant-mediated transport. Glob. Change Biol. 5 (4), 433–440.

Kirschke, S., et al., 2013. Three decades of global methane sources and sinks. Nat. Geosci. 6 (10), 813–823.

Kljun, N., Calanca, P., Rotach, M.W., Schmid, H.P., 2004. A simple parameterisation for flux footprint predictions. Bound. Layer Meteorol. 112 (3), 503–523.

Kljun, N., Rotach, M.W., Schmid, H.P., 2002. A three-dimensional backward Lagrangian footprint model for a wide range of boundary-layer stratifications. Bound. Layer Meteorol. 103 (2), 205–226.

Kroon, P.S., Schrier-Uijl, A.P., Hensen, A., Veenendaal, E.M., Jonker, H.J.J., 2010. Annual balances of CH4 and N2O from a managed fen meadow using eddy covariance flux measurements. Eur. J. Soil Sci. 61, 773–784.

Lai, D.Y.F., Moore, T.R., Roulet, N.T., 2014. Spatial and temporal variations of methane flux measured by autochambers in a temperate ombrotrophic peatland. J. Geophys. Res. Biogeosci. 119 (5), 864–880.

Le Mer, J., Roger, P., 2001. Production, oxidation, emission and consumption of methane by soils: a review. Eur. J. Soil Biol. 37 (1), 25–50.

Mahrt, L., 2000. Surface heterogeneity and vertical structure of the boundary layer. Bound. Layer Meteorol. 96 (1–2), 33–62.

Matthes, J.H., Sturtevant, C., Verfaillie, J., Knox, S., Baldocchi, D., 2014. Parsing the variability in CH4 flux at a spatially heterogeneous wetland: integrating multiple eddy covariance towers with high-resolution flux footprint analysis. J. Geophys. Res. Biogeosci., 2014JG002642.

Nakai, T., Shimoyama, K., 2012. Ultrasonic anemometer angle of attack errors under turbulent conditions. Agric. For. Meteorol. 162–163 (0), 14–26.

Oren, R., et al., 2006. Estimating the uncertainty in annual net ecosystem carbon exchange: spatial variation in turbulent fluxes and sampling errors in eddy-covariance measurements. Glob. Change Biol. 12 (5), 883–896.

Pattey, E., Strachan, I.B., Desjardins, R.L., Massheder, J., 2002. Measuring nighttime CO2 flux over terrestrial ecosystems using eddy covariance and nocturnal boundary layer methods. Agric. For. Meteorol. 113 (1–4), 145–158.

Pattey, E., Trzcinski, M.K., Desjardins, R.L., 2005. Quantifying the reduction of greenhouse gas emissions as a result of composting dairy and beef cattle manure. Nutr. Cycl. Agroecosyst. 72 (2), 173–187.

Peltola, O., et al., 2014. Evaluating the performance of commonly used gas analysers for methane eddy covariance flux measurements: the InGOS inter-comparison field experiment. Biogeosciences 11 (12), 3163–3186.

Peltola, O., Mammarella, I., Haapanala, S., Burba, G., Vesala, T., 2013. Field intercomparison of four methane gas analyzers suitable for eddy covariance flux measurements. Biogeosciences 10 (6), 3749–3765.

Rannik, Ü., et al., 2012. Footprint analysis. In: Aubinet, M., Vesala, T., Papale, D. (Eds.), Eddy Covariance. Springer Atmospheric Sciences, Springer Netherlands, pp. 211–261.

Rannik, Ü., Vesala, T., 1999. Autoregressive filtering versus linear detrending in estimation of fluxes by the eddy covariance method. Bound. Layer Meteorol. 91 (2), 259–280.

Rinne, J., et al., 2007. Annual cycle of methane emission from a boreal fen measured by the eddy covariance technique. Tellus B 59 (3), 449–457.

Schrier-Uijl, A., et al., 2010a. Methane emissions in two drained peat agro-ecosystems with high and low agricultural intensity. Plant Soil 329 (1–2), 509–520.

Schrier-Uijl, A.P., et al., 2010b. Comparison of chamber and eddy covariance-based CO2 and CH4 emission estimates in a heterogeneous grass ecosystem on peat. Agric. For. Meteorol. 150 (6), 825–831.

Schulze, E.D., et al., 2009. Importance of methane and nitrous oxide for Europe's terrestrial greenhouse-gas balance. Nat. Geosci. 2 (12), 842–850.

Schäfer, C.M., Elsgaard, L., Hoffmann, C.C., Petersen, S.O., 2012. Seasonal methane dynamics in three temperate grasslands on peat. Plant Soil 357 (1–2), 339–353.

Sun, F., et al., 2010. Partitioning the variance between space and time. Geophys. Res. Lett. 37 (12), L12704.

Teh, Y., et al., 2011. Large greenhouse gas emissions from a temperate peatland pasture. Ecosystems 14 (2), 311–325.

Tokida, T., et al., 2007. Falling atmospheric pressure as a trigger for methane ebullition from peatland. Glob. Biogeochem. Cycles 21 (2), GB2003.

Van Ulden, A.P., Wieringa, J., 1996. Atmospheric boundary layer research at Cabauw. Bound. Layer Meteorol. 78 (1–2), 39–69.

Whiting, G.J., Chanton, J.P., 1993. Primary production control of methane emission from wetlands. Nature 364 (6440), 794–795.

Vickers, D., Mahrt, L., 1997. Quality control and flux sampling problems for tower and aircraft data. J. Atmos. Ocean. Technol. 14 (3), 512–526.

Wilks, D.S., 2006. Statistical Methods in the Atmospheric Sciences, International Geophysics Series. Academic Press, Amsterdam, ISSN 0074-6142; 91, xvii, 627 s pp.

Winderlich, J., Gerbig, C., Kolle, O., Heimann, M., 2014. Inferences from CO_2 and CH_4 concentration profiles at the Zotino Tall Tower Observatory (ZOTTO) on regional summertime ecosystem fluxes. Biogeosciences 11 (7), 2055–2068.

Wösten, J.H.M., Veerman, G.J., de Groot, W.J.M., Stolte, J., 2001. Waterretentie- en doorlatendheidskarakteristieken van boven- en ondergronden in Nederland: de Staringreeks. Vernieuwde uitgave 2001, Alterra. Research Instituut voor de Groene Ruimte, Wageningen.

Yvon-Durocher, G., et al., 2014. Methane fluxes show consistent temperature dependence across microbial to ecosystem scales. Nature 507 (7493), 488.

Zhu, X., Zhuang, Q., Lu, X., Song, L., 2014. Spatial scale-dependent land–atmospheric methane exchanges in the northern high latitudes from 1993 to 2004. Biogeosciences 11 (7), 1693–1704.